Various Considerations on Seismic Disaster Prevention for Earthquakes at Central Italy

Yutaka Nakamura[1], Jun Saita[1] and Tsutomu Sato[1]

Abstract

On the earthquake sequence in central Italy from August 24, 2016, here investigates many aspects from the viewpoint of earthquake disaster prevention with opened strong motion records. Additionally the other earthquake sequence in central Italy from September 26, 1997 was also investigated. As a result, it is cleared that EEW, Earthquake Early Warning, can get a time margin from a few seconds to 10 seconds at the best. It is extremely important for making not so long time margin of EEW to make advance preparation as ensuring safety zone and to carry out evacuation training. On the source location which is one of the earthquake information to determine the damaged area, it can be fixed a few seconds after the first earthquake detection. And the source of the maximum earthquake motion is investigated and it is confirmed that it can be possibly determined within 30 seconds after the first detection. Additionally a severe damage is estimated around the area of fault rupture. Judgement whether near the fault or not can be adopted the size of the permanent deformation of the crust, and this permanent deformation can be estimated from double integration of the observed acceleration waveform. This knowledge is considered to support an available quick response to determine the damaged area immediately after an earthquake occurrence. From the result of the microtremor measurement after the 1997 earthquake, the anti-seismicity of the structure as residences is estimated to have important effect. Here reinforcement against earthquakes must be emphasized to be the most important for the earthquake disaster prevention.

---

1 System and Data Research, Tokyo, Japan.

1. Introduction

In September 1997, a *Mw* 6.0 Earthquake occurred at central Italy and *Basilica di San Francesco* in Assisi suffered damage as collapsing a part of the ceiling. This basilica had been attacked by a relative large foreshock nine hours before and suffered damage as falling down of the mural paintings. During the investigation of the damage situation by cultural property officials, the main shock attacked this basilica. There was some villages completely damaged in the epicentral area by these earthquakes, and the damage situation was similar to that caused by the earthquakes in central Italy after August 2016. A microtremor measurement was conducted in November 1997 at villages in the epicentral area. The result suggested that the dynamic characteristics of the structures were the main cause of the damage although there was a certain level of relation between the ground condition and the damage. In case of the series of the damage earthquakes in 2016, catastrophic damage was caused in Amatrice, a little far from the epicenter, although no significant damage was caused in Norcia, almost same distance from the epicenter as Amatrice. It was cleared that structures in Norcia have been enhanced earthquake safety by seismic reinforcement following the past experience, and it indicates clearly that the enhancing the earthquake safety has a profound effect for reducing the earthquake damage. After that, the largest event occurred close to Norcia and caused serious damage for Norcia. However most of the local people had understood the characteristics that large earthquakes always come in sequence in central Italy and had already evacuated, so it is reported that the human suffering was relative few. Here considers on the earthquake disaster prevention with opened strong motion records, specifically, as earthquake early warning simulation for the time margin against sudden earthquakes, quick determination of the epicenter for rapid damage estimation, process of seismic intensity or calculation of the scale of the crustal deformation.

2. Realtime seismic intensity and the alarm timing

2.1. On the realtime seismic intensity

The realtime seismic intensity, *RI*, can be summarized as following. The realtime seismic intensity is physically an index relating to the capacity of supplying earthquake energy and defined as follows ([2],[4],[5]);

$$RI = \log(PD) + 6.4$$
$$PD = \boldsymbol{a} \cdot \boldsymbol{v}$$

Here, $\boldsymbol{a}$ and $\boldsymbol{v}$ are acceleration vector and velocity vector of the earthquake motion on the ground surface, respectively, and an operator, " $\cdot$ ", indicates inner product. The constant term is put to fit *RI* to instrumental seismic intensity by JMA, Japan Meteorological Agency, and defined when the both vector are in MKS unit (m/s^2, m/s). In case of the unit in Gal (cm/s^2) and kine (cm/s) for both vectors, the constant term will be 2.4. Also, the instrumental seismic intensity by JMA is derived from an acceleration waveform of 60 seconds after earthquake detection aiming to fit the past earthquake intensity scale based on the feeling of human. Although this index is an artificial index basically derived from the maximum acceleration with the predominant frequency and other items with more than 60 seconds after the earthquake detection, it has been entrenched as an instrumental seismic intensity in Japan.

Power Density *PD* in W/kg is a power density of an earthquake motion and defined as an earthquake motion power acting on a unit mass. Following the definition, a large seismic intensity means that there is a potential leading to destruction with supplying large energy with an object in absorbing easily energy as resonance. It is important to understand this index as one of the indices measuring the earthquake motion on the context of the earthquake damage, as acceleration relating to force, velocity relating to strain or energy, or displacement relating to deformation.

The seismic intensity corresponding to a power density *PD* = 1 W/kg is 6.4 for *RI* or 10.6 for *MMI*. Additionally, a human activity can also be expressed with *PD*. A basal metabolism of a human body is said to be about 1 W/kg and an activity metabolism transiently reaches around 10 W/kg during exercise as swimming or football. In case of a flat house, the mass act an earthquake load seems to be about

5 tons at the roof and it corresponds to a body weight of 70 persons when assuming 70 kg for one person. For this house, the power of the earthquake motion of seismic intensity 6.4 is same as the power when 70 persons exercise in 1 W/kg. A motion of 1 W/kg is equal to a motion bringing up the human body itself to 10 cm per second.

So, the physical meaning of *RI* 6.4 is an earthquake motion having a potential to supply a power as bringing up this house to 10 cm per second. When an earthquake motion of *RI* 6.4 acts in this house for one second, the act earthquake motion energy is equivalent of a potential energy for 10 cm and a velocity corresponding to the motion becomes considerably large as 1.4 m/s. It can be easily imagined that the house absorbing this energy faces collapse if it is not constructed firm enough. This maximum energy can be supplied by the earthquake motion of *RI* 6.4 even for one second. The longer acts, the larger a power supplied. A vulnerable structure will be collapsed if the structure receives directly this earthquake energy.

It is found to avoid collapse that the countermeasures are required as proofing of a structure against large deformation energy (earthquake resistant), avoiding resonance (vibration control), converting supplied power to the other as heat immediately before causing strain energy (vibration damper), or avoid transmitting the earthquake motion to a structure (seismic isolation).

Because the realtime intensity *RI* with physical background is quite characteristic of sudden increase from a level of microtremor when arriving an earthquake motion, it can steadily detect an earthquake and it is easy to read certainly the detection time. And *RI* is expected to have high affinity to the other intensities based on the human feeling. Here makes various considerations using these characteristics.

Also, conversion from *RI* to *MMI*, the Modified Mercalli Intensity, uses a following formula ([7]).

$$MMI = RI \times \frac{11}{7} + 0.5$$

2.2. Variation of the realtime intensity RI and timing of issuing alarm in central Italy

Seismic motion records of some strong motion observatories at epicentral area of following events are overviewed from the realtime intensity *RI* using the opened strong motion record by Italian strong motion observation network ITACA (http://itaca.mi.ingv.it/ItacaNet/).

#1: A *Mw* 6.0 and depth 8.1 km earthquake on August 24, 2016, caused catastrophic collapse for Amatrice and other village.
#2: A *Mw* 5.9 and depth 7.5 km earthquake on October 26, 2016, caused damage around Visso and other village.
#3: A *Mw* 6.5 and depth 9.4 km earthquake on October 30, 2016, caused damage around Norcia and other town.
#4: A *Mw* 6.0 and depth 5.7 km main shock (#4m) and a *Mw* 5.7 and depth 5.7 km foreshock (#4f) on September 26, 1997, caused damage as partially falling down of the mural paintings of *Basilica di San Francesco* in Assisi by Event #4f and as collapsing two parts of the ceiling of the basilica with damage for villages around the epicentral area by Event #4m 9 hours later.
(All magnitude *Mw* and depth are estimated by INGV.)

Figure 1 shows the distribution of these epicenters and strong motion observatories for this analysis.

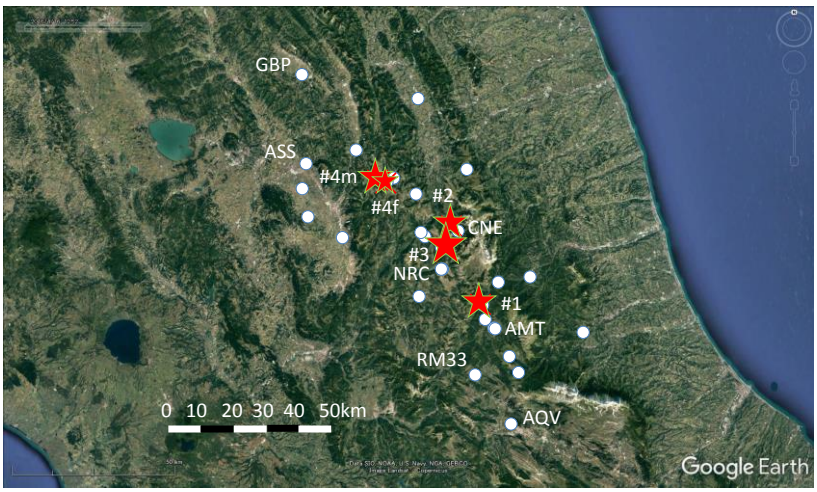

Figure 1. Location of epicenters and strong motion observatories described in this paper

Figures 2 to 5 show change in time of the realtime intensity *RI* based on strong motion records of these earthquakes. Because the recorded time seems to be almost exact except the 1997 earthquakes, these figures show the change of the realtime intensity *RI* to the absolute time. All the figures are for 25 seconds length to compare a sharpness of rising and other items for each other. In case of the 1997 earthquakes, the absolute time is uncertain and the record did not include the P wave initial motion for most of the station. So the starting time of the record is estimated as dividing a hypo-central distance by the S wave velocity assuming 3.5 km/s and then subtracting a time between the recording starting time and the S wave arriving time. In this way, the changing situation of the realtime intensity *RI* at each station is indicated on the time scale in the same manner, and it is possible to compare with all the diagrams.

The sharpness of rising the realtime intensity *RI* is not quite differ from the events or the stations. Of course the sharpness of rising is kept till large seismic intensity in case of a large earthquake and is kept till only small seismic intensity at distant stations. Therefore, a rise sometimes becomes gradual in appearance because the sharp rising is buried in noise depending on the noise level. This means, it is

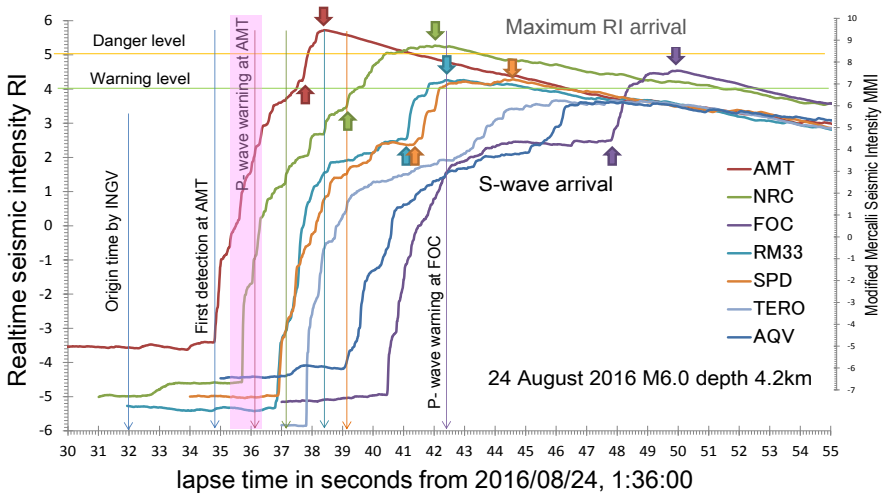

Figure 2. Change of the realtime seismic intensity at some sites with the timing of P-wave warning (long downward arrows, pink band emphasizing the first alarm) based on FREQL simulation for Event #1

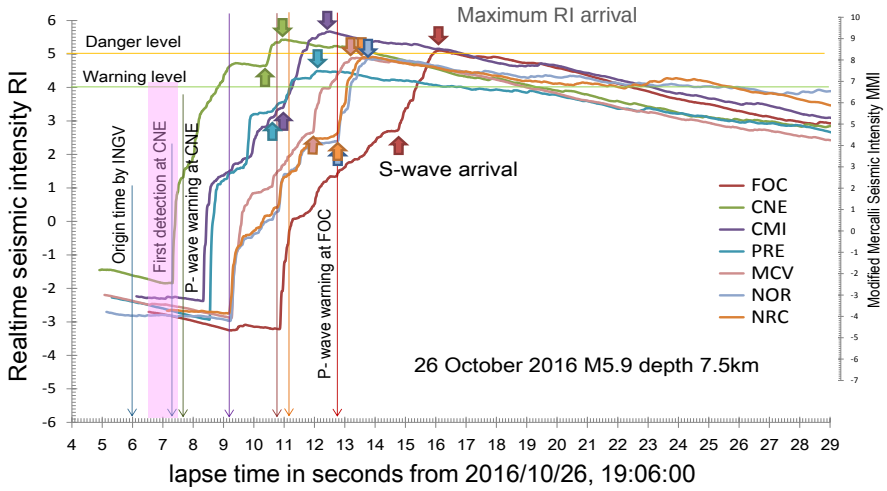

Figure 3. Change of the realtime seismic intensity at some sites and the timing of P-wave warning (long downward arrows, pink band emphasizing the first alarm) based on FREQL simulation for Event #2

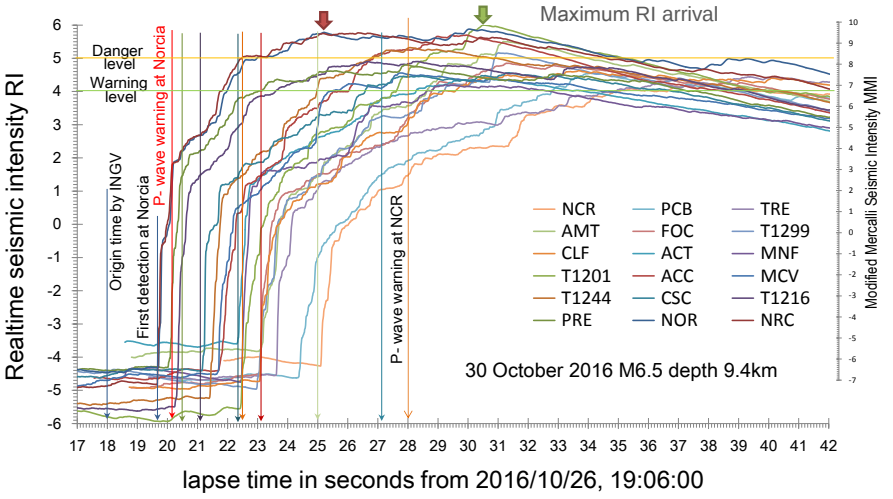

Figure 4. Change of the realtime seismic intensity at some sites and the timing of P-wave warning (long downward arrows, red character and arrow emphasizing the first alarm) based on FREQL simulation for Event #3

necessary to notice that there is a possibility to include serious misunderstandings for evaluation of the distance with sharpness of the rising.

In these figures, there are long thin downdraft arrows as the time of earthquake detection, short fat updraft arrows as the arrival time of S-wave, short fat downdraft arrows as the arrival time of maximum seismic intensity, and green and orange horizontal lines as the level of the seismic intensity *RI* 4 and *RI* 5. Earthquake damage begins experientially to be caused by more than the seismic intensity *RI* 5 in Japan. The level of the seismic intensity *RI* 5 is indicated as a danger level, and also *RI* 4 is indicated as a warning level. Additionally the *MMI* scale is indicated in the right side of the figures for reference.

Event #3 was observed at many sites over the seismic intensity *RI* 5 and its duration time was long. The other events have a few sites over *RI* 5 and their duration time is short. From a viewpoint of the destructive energy, Event #3 is quite larger than the others and this agrees that *Mw* 6.5 for Event #3 is the maximum value among the all analyzed earthquakes.

In case of Event #4m, the realtime intensity *RI* increased gradually at the site GBP and the earthquake motion continues accordingly for a long time. It is estimated that an earthquake motion with long natural

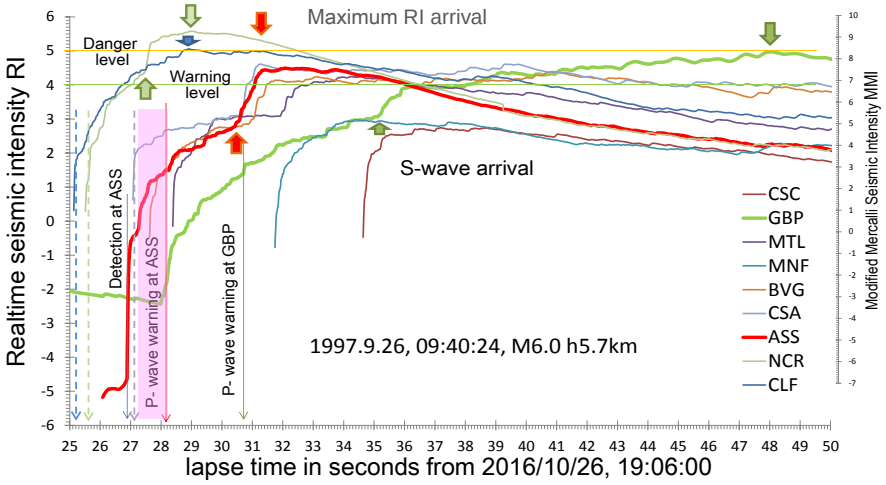

Figure 5. Change of the realtime seismic intensity at some sites and the timing of P-wave warning (long downward arrows , pink band emphasizing the alarm at Assisi) based on FREQL simulation for Event #4m

period may grow gradually in surface ground. However common structures will not resonance with this long period earthquake motion, it may be necessary for a structure with long natural frequency as a high rise building to notice about resonance.

Onsite alarm has about 2 to 5 seconds between issuing alarm and arrival of maximum motion for each station. There is the potential to extend this time up to about 10 seconds in the damaged area excepting a first few sites if these stations can be connected via network and the alarm at the first detection site can be participated. A time margin at damaged area caused by earthquake sequence in central Italy is a few to 10 seconds anyway at most, and it is necessary for making valuable to take applicable countermeasures of hardware as constructing safety zone and to carry out the evacuation training. It must be anew emphasized that to ensure the earthquake resistance is basic of the earthquake disaster prevention.

The realtime seismic intensity sometimes suddenly increases after the earthquake motion arrival, or sometimes changes as divided for some small part with sharp but small rising. It is estimated that the change of realtime seismic intensity is corresponding to slip situation of a fault. Anyway it will be important for the earthquake disaster prevention to make residences tenacious avoiding sudden collapse.

Event #1 caused catastrophic damage for Amatrice. The maximum realtime seismic intensity *RI* was 5.7 corresponding to *MMI* 9.5 from a strong motion record at a station AMT close to Amatrice, and this is a relatively serious situation as possibly suffering some sort of damage in Japan. AMT is the nearest site to epicenter of INGV with epicentral distance 8.5 km. At the second nearest site NRC with epicentral distance 15.3 km, *RI* was 5.3 corresponding to *MMI* 8.8, and it was small a lot for that of AMT. It is said that there was little damage as no death at that village Norcia. Earthquake retrofit had been conducted there and this seems to be the effect of the work in addition to lower *RI* than AMT.

Seismic capacity of structures may vary considerably for areas in Italy. It seems that it is important for Italy remaining a lot of traditional old structures to grasp the vulnerability of structures individually and make a suitable reinforcement as well as to grasp the ground characteristics. There should be an urgent need to proceed a health investi-

gation of structures utilizing the microtremor measurement and then establish the proper aseismic reinforcement.

3. Distance attenuation of maximum acceleration

Figures 7 to 11 show maximum acceleration of each earthquakes against each epicentral distance. An orange line indicates the acceleration at the base ground estimated from strong motion records along the first bullet train Tokaido Shinkansen line in Japan.

This is an estimation of acceleration considering two kinds of attenuation as geometric and distance (or inner) attenuation as followings;

$$\mathrm{A} = A_0 \times e^{-\alpha\Delta}/\Delta^n$$

Assuming n=0.5 from geometric attenuation of the surface wave, the constants are defined statistically from earthquakes recorded by SMAC type seismometer installed for Shinkansen line, then the relationship between the constants and magnitude for many events, and finally the formula below can be obtained ([1]). Also, the term $\log_{10}(\Delta + h)$, here h is depth in km, is used instead of $\log_{10}\Delta$ not only to avoid the abnormity at the epicentral area ($\Delta \fallingdotseq 0$ km) but also to take account of depth effect. Additionally, the maximum acceleration of this formula has characteristics same as the waveform recorded by the SMAC type seismometer, corresponding to 5HzPGA.

$$\log_{10} A = 0.168 \times M - 0.5 \times \log_{10}(\Delta + h) - 0.0551 \times 10^{-0.156M} \times \Delta + 1.86$$

Figure 6 shows the attenuation curve of 5HzPGA of the Kumamoto earthquake (*Mw* 7.0, *h*=12km) at the central Kyushu island of Japan on April 16, 2016. Blue and orange dots in this figure indicate 5HzPGA observed on the ground surface and under the ground at least 100 m depth, respectively. The acceleration value derived from the formula above corresponds to a lower limit of 5HzPGA on the surface ground shown as the orange curve.

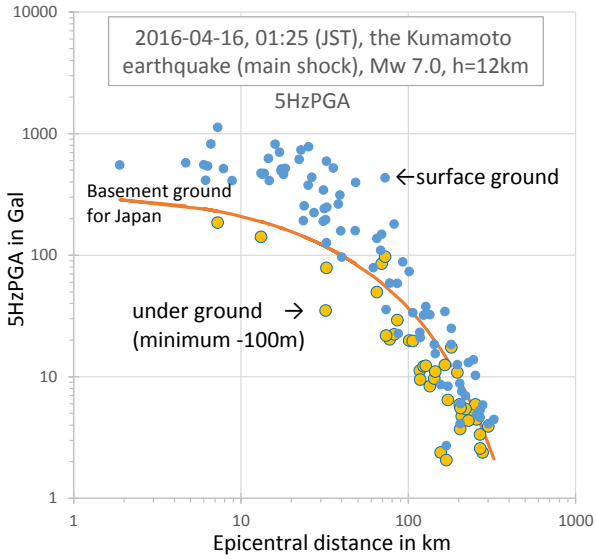

Figure 6. Attenuation curve of 5HzPGA, PGA limited by a frequency range between 0.1Hz and 5Hz for the 2016 Kumamoto earthquake Mw7.0 (main shock)

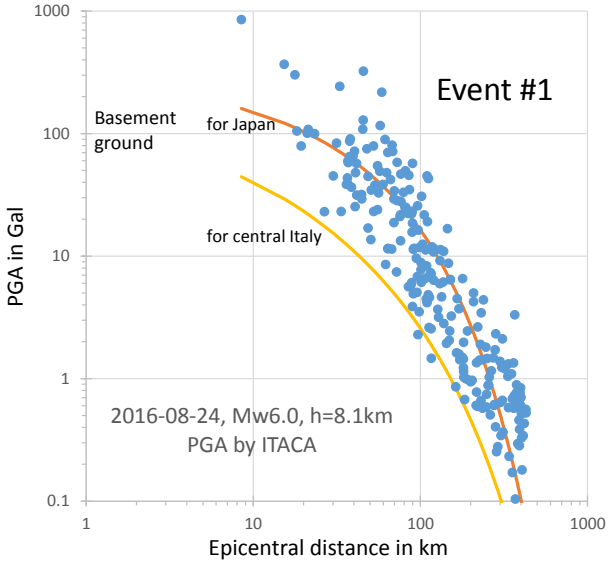

Figure 7. Attenuation curve of PGA for Event #1

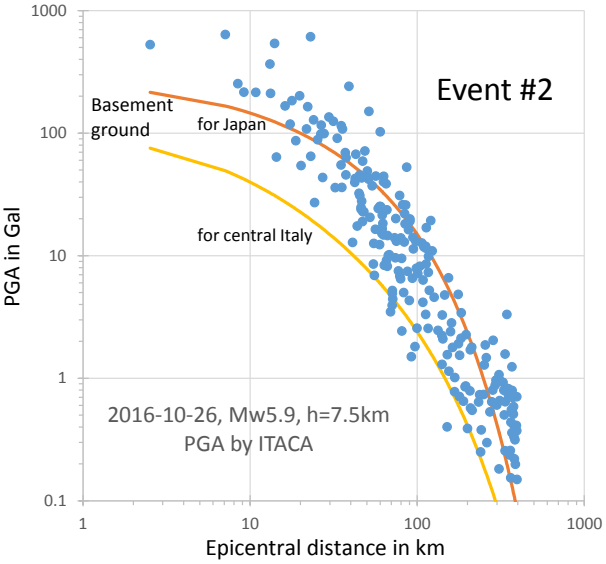

Figure 8. Attenuation curve of PGA for Event #2

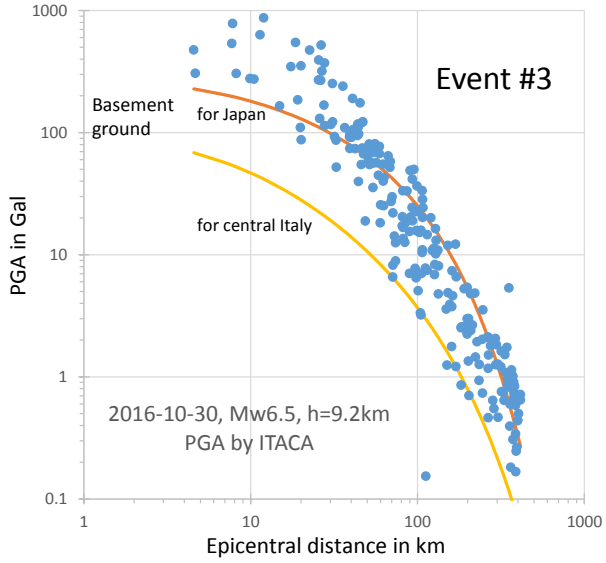

Figure 9. Attenuation curve of PGA for Event #3

On the other hand, PGA becomes significantly larger than 5HzPGA in general. Nevertheless, the distance attenuation situation of observed PGA in Italy shown in Figures 7 to 11 indicates that 5HzPGA derived from the formula above becomes quite larger than the lower limit of the observed PGA. Thus, it is confirmed that PGA in Italy is quite smaller than 5HzPGA in Japan. This smaller maximum acceleration than that commonly in Japan suggests that the ground in Italy is considerably harder than that in Japan.

Therefore, the PGA attenuation curve corresponding to the lower limit of observed PGA in Italy was tried to be derived with arranging the damping term of the formula above. Although the formula above assumes the geometric attenuation of the surface wave, the attenuation situation of PGA in Italy is seems to be proper to apply a geometric attenuation of the body wave. So the constant 0.5 of the formula above is changed for 1.0. The formula below is derived after a simple trial and error process on the constant and the inner attenuation effect for the lower limit of PGA.

$$\log_{10} A = 0.168 \times M - 1.0 \times \log_{10}(\Delta + h) - 0.04 \times 10^{-0.156M} \times \Delta + 1.90$$

Distance attenuation diagram of PGA for each earthquake indicates both attenuation curves in Figures 7 to 11. Estimated PGA from above formula can be confirmed to provide approximately the lower limit of

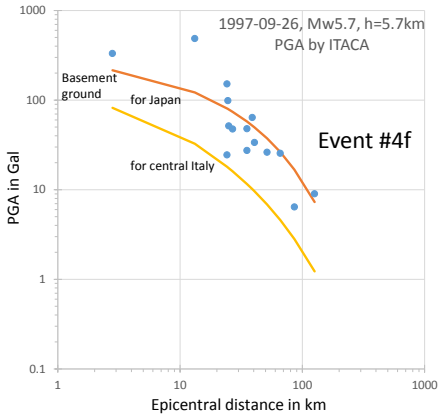

Figure 10. Attenuation curve of PGA for Event #4f

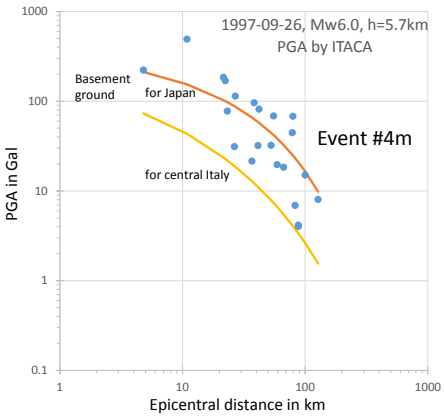

Figure 11. Attenuation curve of PGA for Event #4m

observed PGA for each earthquake.

Evaluating the lower limit of each earthquake as the maximum acceleration at the base ground, the amplification factor of the maximum acceleration is calculated for each sites. This result is compared with the site classification of EC8, Euro Code 8, or the amplification factor derived from HVSR, H/V spectral ratio, of strong motion records as Figures 12 and 13.

Although there is not much correlation between EC8 site classification and estimated amplification factor, the estimated amplification factor clearly correlates with that derived from HVSR.

Apparent amplification factor of the maximum acceleration commonly differs from the amplification factor as so-called site characteristics. However it is not completely unrelated, it must show some relationship. Figure 12 shows this and suggests the amplification factor estimated from HVSR is reasonable.

Here, although it is not paid much attention, it must be noticed that uncorrelated condition between H and V is a precondition in case of discussion on a peak of HVSR about the predominant frequency.

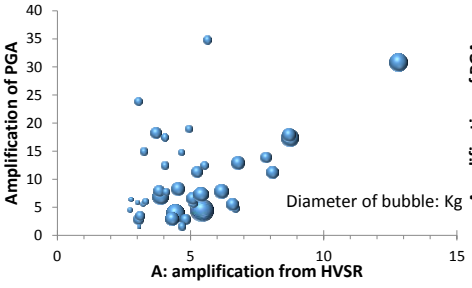

Figure 12. Relationship between amplification of PGA and HVSR, H/V spectral ratio

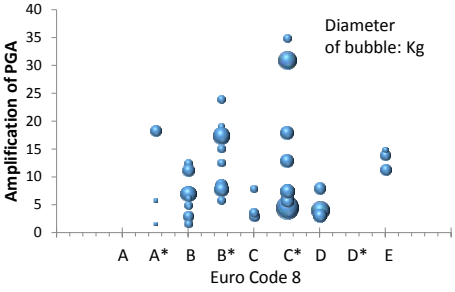

Figure 13. Relationship between amplification of PGA and Euro Code 8

4. A permanent displacement and a vibration displacement derived from the double integration of the strong motion records

Here considers the displacement derived from the double integration of the strong motion records. This displacement includes a

permanent displacement of crust caused by a fault motion and a vibration motion. Because a fault slips around 1 m with a *Mw* 6 class earthquake, a permanent displacement corresponding to this fault motion and a vibration displacement caused by a propagation of an earthquake motion are observed near the fault.

Nonlinear behavior of a ground sometimes can be found depending on the largeness of a strain on the ground. It is also possible to decide a positional relationship roughly between the fault and observation point from the largeness of the permanent displacement. Additionally, this displacement is expected to be utilized for judgement of damage occurrence because the permanent displacement becomes more than some tens cm in case of the site close to the fault.

Figures 14 and 15 show displacement records at some sites for each events, and locus on the map for Event #3, respectively. The permanent displacement was small less than 10 cm for Events #1 and #2, and it seems that the observation stations did not locate close to the epicenter. Event #3 caused a permanent displacement of 40 cm at Norcia and it suggests that this site locates close to the epicenter. In

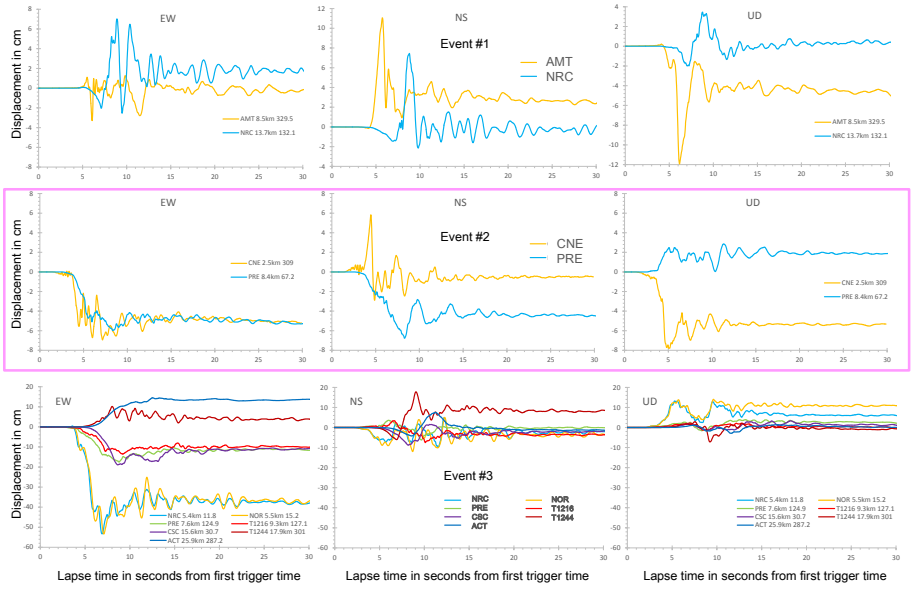

Figure 14. Displacements derived from the double integration of the strong motion for Events #1 to #3

addition, the permanent displacement of this earthquake moves to east at the eastern side and to west at the western side, and it shows the characteristics of the fault motion at this area. This permanent displacement agrees with an observation result of GPS and it is expected that the double integration of a strong motion record can grasp the proper displacement nearly in realtime in case of the displacement at least more than 10 cm. It will be available for the disaster prevention if the damaged area can be determined quickly.

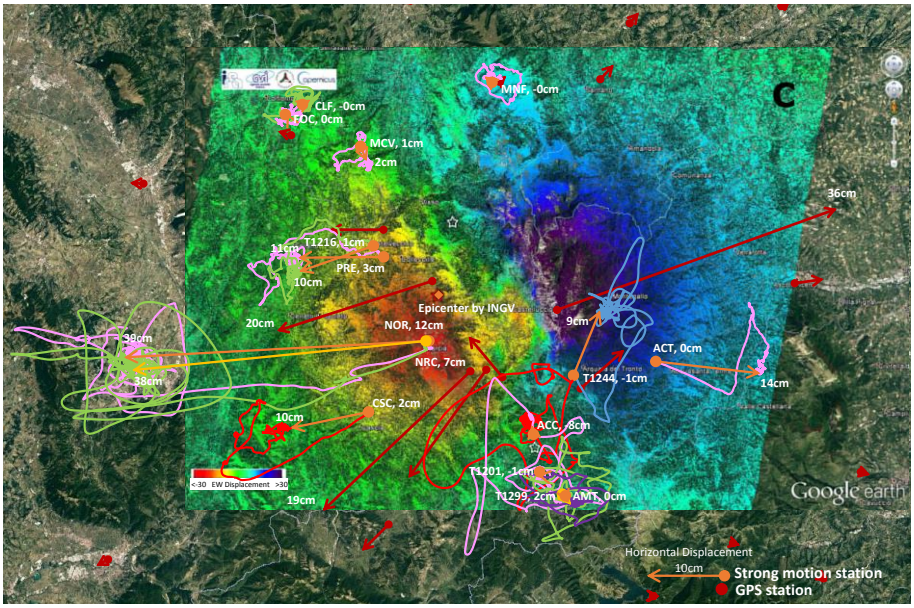

Figure15. Locus of horizontal displacements derived from double integration of strong motion records on a map of displacement distribution by InSAR as red to blue for westward to eastward displacement of EW direction, comparing with displacements by GPS, for Event #3

5. Quick estimation of the epicenter for the damaged area determination

Information of an epicenter of occurred earthquake is important to determine the damaged area. Although the epicenter is commonly the starting point of fault rupture and it mostly differs from an area

concentrating damage, it has already been known that the location of the epicenter can be determined with fairly quickness and accuracy if observation points are installed properly. On the other hand, a source of the earthquake wave causing the maximum motion, hereafter "Max source", is expected to have good correlation with the damaged area. Here considers that how quick the epicenter, the starting point of the fault, and the Max source are determined for Events #1 to #3 given accurate absolute time.

Calculation of an epicenter is to fix five unknowns as the coordination X, Y and Z of the epicenter, the origin time and the wave propagation velocity using the time of commencement of each station by the least squares method. Here the wave propagation velocity is given as known and the rounded coordination of the first detection site is set as initial value. The result is given as a value within a predetermined error as 0.5 km after repeatedly calculation. The starting point of the fault rupture uses the P wave rising time as the rising of the realtime seismic intensity. Additionally, the P wave propagation velocity is set 6 km/s. Estimation of the Max source uses a time of maximum realtime seismic intensity, and earlier time is used if the maximum value is observed repeatedly. The wave propagation velocity for the Max source estimation is basically set to 4 km/s and decreased in step of 0.1 km/s with lower limit of 3.5 km/s.

Figures 16 to 18 show the result of calculation as mentioned above. And Tables 1 to 3 list the appearance time of the P wave and the maximum value. Tables 4 to 6 list the results of estimated hypocenter and that by INGV and USGS.

It is confirmed from the result of calculation that the hypocenter as the starting point of the fault rupture can be determined with wave arrival time of the first five sites with considerable accuracy. From this result, it is expected to determine correctly the location of the starting point of the fault rapture with the first five sites of detecting an event, of course although it is depends on the relationship between the epicenter and the observation stations. In case of Event #1, the fifth station detected the earthquake motion 2.1 seconds after the detection of the first station on the time series. Because it takes less than 0.1 seconds for the calculation of the hypocenter, it is possible to determine the correct location of the hypocenter in a little over two

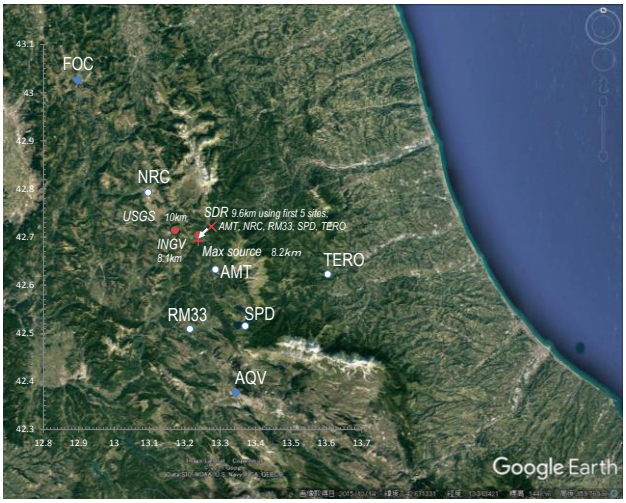

Figure 16. Quick estimation results of the hypocenter and Max source showing depth in km, with hypocenter estimation by INGV and USGS for Event #1.

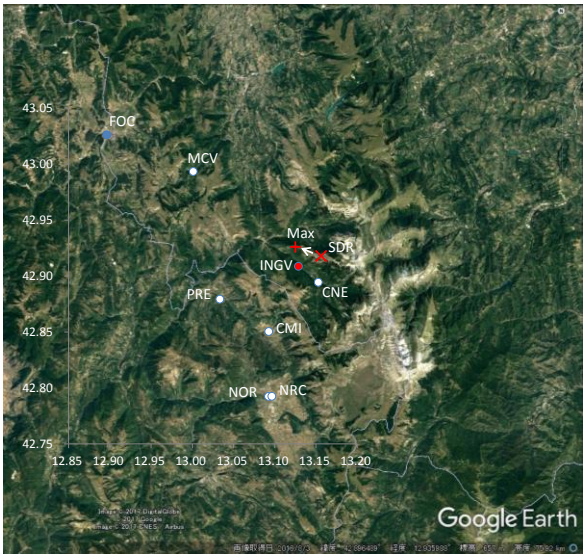

Figure 17. Quick estimation results of the hypocenter and Max source with hypocenter estimation by INGV for Event #2.

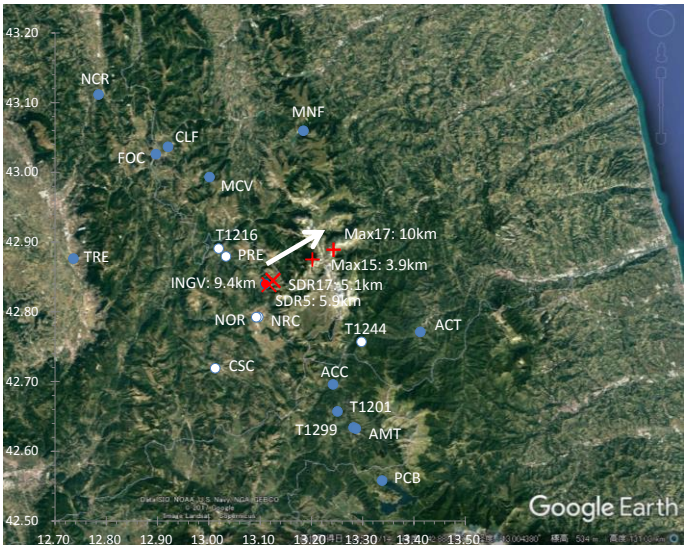

Figure 18. Quick estimation results of the hypocenter and Max source with hypocenter estimation by INGV for Event #3. A number after colon means depth in km.

Table 1. Appearance time of the P wave and the maximum RI at strong motion sites for Event #1

	arrival time						
site	AMT	NRC	TERO	RM33	SPD	AQV	FOC
N (degree)	42.6325	42.7925	42.62279	42.50898	42.515099	42.377102	43.026299
E (degree)	13.2866	13.0964	13.60393	13.21452	13.371	13.3439	12.8965
p-time	34.80	35.70	37.60	36.80	36.90	39.03	40.45
max-time	38.40	42.10	45.80	42.50	44.60	47.30	50.00
	note: times are lapse time in seconds from 2016/08/24, 01:31:00						

Table 2. Appearance time of the P wave and the maximum RI at strong motion sites for Event #2

	arrival time						
site	NOR	MCV	FOC	CNE	PRE	NRC	CMI
N (degree)	42.792442	42.993401	43.0263	42.894402	42.879299	42.792543	42.850399
E (degree)	13.092422	13.0013	12.896506	13.1528	13.0334	13.096475	13.0928
p-time	9.23	9.28	10.86	7.34	8.56	9.20	8.34
max-time	13.80	13.20	16.10	11.00	12.10	13.70	12.50
	note: times are lapse time in seconds from 2016/10/26, 19:18:00						

Table 3. Appearance time of the P wave and the maximum RI at strong motion sites for Event #3

	arrival time																	
site	NRC	NOR	PRE	T1216	CSC	T1244	MCV	ACC	T1201	MNF	ACT	CLF	T1299	FOC	AMT	TRE	PCB	NCR
N (degree)	42.7925	42.7924	42.8793	42.8907	42.7191	42.7570	42.9934	42.6960	42.6573	43.0597	42.7713	43.0367	42.6342	43.0263	42.6325	42.8765	42.5580	43.1116
E (degree)	13.0965	13.0924	13.0334	13.0190	13.0123	13.2978	13.0013	13.2420	13.2508	13.1845	13.4125	12.9204	13.2822	12.8965	13.2866	12.7358	13.3380	12.7847
p-time	19.68	19.71	20.03	22.25	21.17	21.41	21.71	21.71	22.44	22.47	22.31	23.08	22.98	23.07	23.19	23.62	24.39	25.11
max-time	25.30	30.00	27.90	28.20	31.30	28.20	27.90	29.80	30.50	29.20	30.00	33.90	31.10	31.40	31.30	39.30	34.10	37.10
	note: times are lapse time in seconds from 2016/10/30, 06:40:00																	

Table 4. Estimated hypocenter and Max source with the hypocenter by INGV and USGS for Event #1

	source parameter				cf.	
estimated by	SDR	SDR	SDR	SDR	INVG	USGS
	hypocenter	hypocenter	Max source	Max source	hypocenter	hypocenter
site number/ Mw	5	7	5	7	M6.0	M6.2
N (degree)	42.722	42.717	42.690	42.692	42.698	42.714
E (degree)	13.275	13.274	13.246	13.238	13.234	13.172
depth in km	9.6	9.6	8.2	6.2	8.1	10.0
origin time	32.5	32.5	38.9	38.6	32.0	
assumed v	vp=6km/s	vp=6km/s	vs=3.7km/s	vs=3.8km/s		
note: times are lapse time in seconds from 2016/08/24, 01:31:00						

Table 5. Estimated hypocenter and Max source with the hypocenter by INGV for Event #2

	source parameter				cf.
estimated by	SDR	SDR	SDR	SDR	INGV
	hypocenter	hypocenter	Max source	Max source	hypocenter
site number/ Mw	5	6	5	6	Mw 5.9
N (degree)	42.918	42.917	42.926	42.921	42.9087
E (degree)	13.156	13.154	13.125	13.123	13.1288
depth in km	2.7	2.5	3.0	2.2	7.5
origin time	6.7	6.8	9.7	9.8	6.0
assumed v	vp=6km/s	vp=6km/s	vs=3.7km/s	vs=3.6km/s	
note1: times are lapse time in seconds from 2016/10/26, 19:18:00					
note2: NOR and NRC are considered as one site because they are closed for each other.					

Table 6. Estimated hypocenter and Max source with the hypocenter by INGV for Event #3

	source parameter				cf.
estimated by	SDR	SDR	SDR	SDR	INGV
	hypocenter	hypocenter	Max source	Max source	hypocenter
site number/ Mw	5	17	15	17	Mw 6.5
N (degree)	42.839	42.845	42.875	42.889	42.840
E (degree)	13.117	13.125	13.202	13.243	13.110
depth in km	5.9	5.1	3.9	10.0	9.4
origin time	18.3	18.4	25.9	25.4	18.0
assumed v	vp=6km/s	vp=6km/s	vs=3.6km/s	vs=3.5km/s	
note1: times are lapse time in seconds from 2016/10/30, 06:40:00					
note2: NOR and NRC are considered as one site because they are closed for each other.					

seconds after first detection under a situation gathering entire data in realtime. It was 1.89 seconds and 1.73 seconds after the first detection to get the detection time of the whole five stations for Events #2 and #3, respectively. Therefore, it is expected that the hypocenter as the starting point of the fault rapture can be determined about two seconds after the first earthquake detection for this central Italy earthquake sequence. And the magnitude of the earthquake will be able to be estimated immediately after the hypocenter determination.

On the Max source, it is determined with the data of five or seven stations for Event #1 assuming the wave propagation velocity as 3.7 or 3.8 km/s. Although it seems that it requires certain time to confirm the appearance time of the maximum realtime seismic intensity, assuming the required time as 10 seconds, the Max source will be determined 21.0 or 25.2 seconds later from the first detecting with fixing the appearance time of the maximum realtime seismic intensity. Similarly, the appearance time of the five or six stations were fixed 16.3 or 18.8 seconds and the Max source was estimated with the wave propagation velocity of 3.7 or 3.6 km/s for Event #2. In case of Event #3, after fixing the appearance time of 17 stations, the Max source was determined at about 10 km north-east of the epicenter with the wave propagation velocity of 3.5 km/s. The time of determination seemed to be about 30 seconds after the first detection time. This Max source locates at the northern edge of a seismic gap of aftershocks about 10 km east from the epicenter as shown in Figure 19. If the seismic gap of aftershocks corresponds to the rupture zone of the main shock, it is reasonable that the maximum earthquake energy is ejected from the location of the Max source. This means that the Max source agrees with the seismic gap of aftershocks and the validity of the Max source is suggested. An extension of the damage around the Max source is concerned and it will be necessary to verify with the actual situation of damage.

It was found that the hypocenter can be determined accurately within a few seconds after the first earthquake detection as the rough information to determine the damaged area. The Max source considered to have relation to the damage concentrated area, and the time for determination may require about 30 seconds. The Max source will be utilized as a trigger information of an immediate response by a

local department on disaster prevention, although it is late information as an alarm for the damaged area. For this purpose, it is necessary to keep considering about the relationship between the Max source and damaged area or the promptness of estimation.

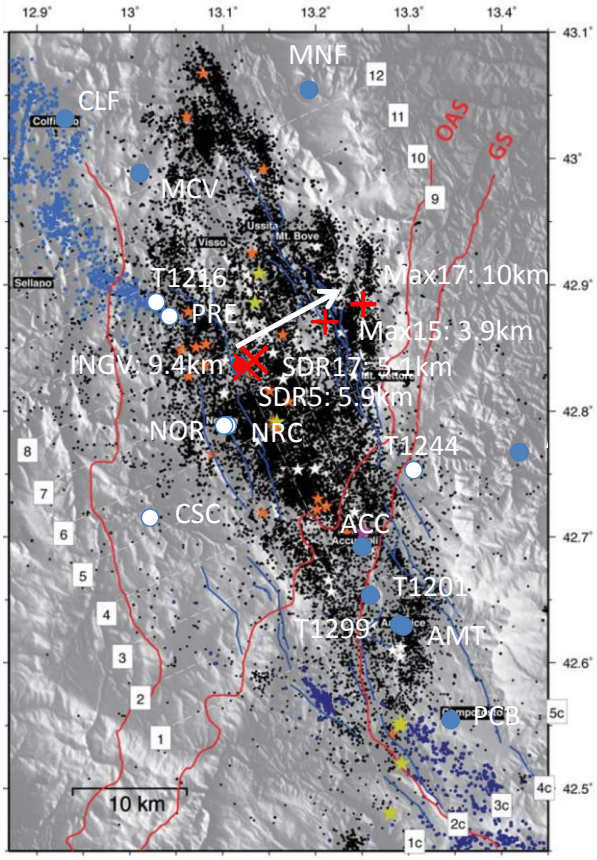

Figure 19. Estimated results on aftershock distribution map for Event #3, adding to Figure 3 of [9]

6. Relationship between damage and earthquake response characteristics of ground and structures

Here describes the result of the microtremor measurement on September 1997 after Event #4 ([3]). The target area of this

measurement was at and around *Basilica di San Francesco* in Assisi collapsed as falling down of ceilings and some damaged villages.

At the basilica, microtremor was measured at totally three points as the floor around the entrance of the lower and upper church and on the remained ceiling backward of the collapsed ceiling near the entrance. A two-story residence was also measured at one points on the first floor. These measurements were conducted individually and not simultaneous at ground and buildings.

Figure 20 shows the location of the microtremor measurement on the ground with damage situation roughly around the point. Figure 21 is H/V spectrum derived from the measured microtremor.

Figure 22 shows *Kg value* derived from the peak frequency and its peak value, amplification factor, of H/V spectrum. However the damage of buildings tends to be caused at the area with large *Kg value*, the value is 10 μstrain/Gal at most and is not so large than usual it is concerned that significant non-linearity of ground must be caused by considerably large earthquake motion and it is estimated that the amplification effect of the earthquake motion is also not so large. Therefore, it seems that the damage occurrence depends considerably on the anti-seismicity of the building itself.

The earthquake response characteristics of the damaged basilica and non-damaged residence using microtremor are shown in Figures 23 and 24. Table 7 is *Kb value* for buildings and *Kb value* is one of *K*

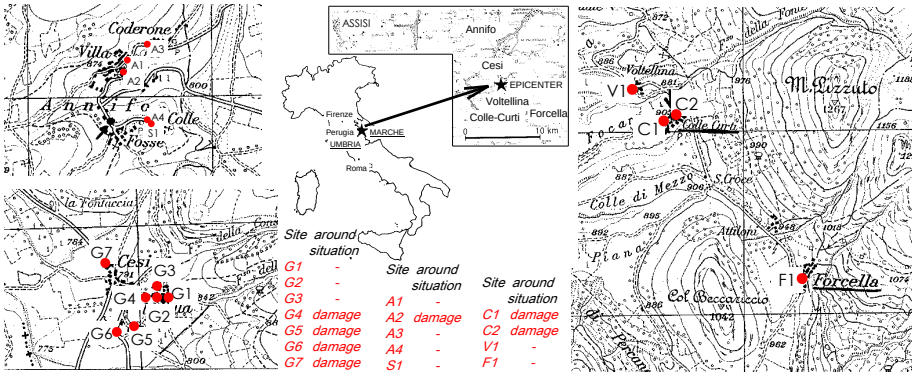

Figure 20. Location of the microtremor measurement points on the ground and a two-story house (S1)

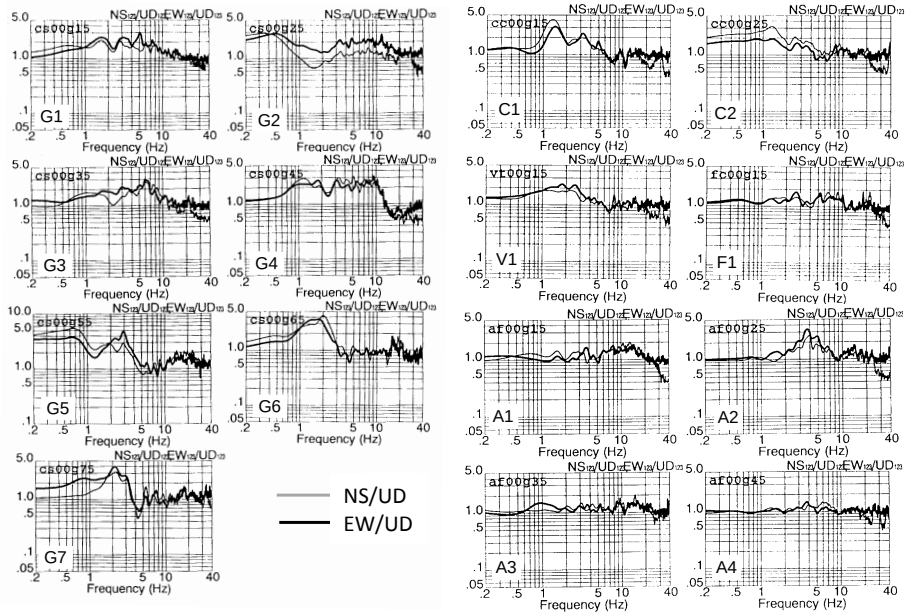

Figure 21. HVSR of microtremor at the measuring sites on the ground

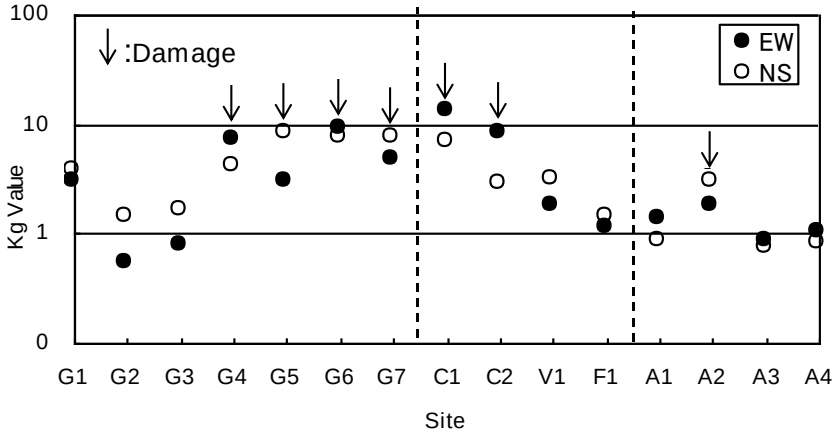

Figure 22. Kg-values derived from HVSR of microtremor

values derived from the earthquake response characteristics above. The earthquake motion at the ground surface was estimated from the record as 150 Gal at Assisi and 100 Gal around the residence considered as the base ground. Although the drift angle is estimated

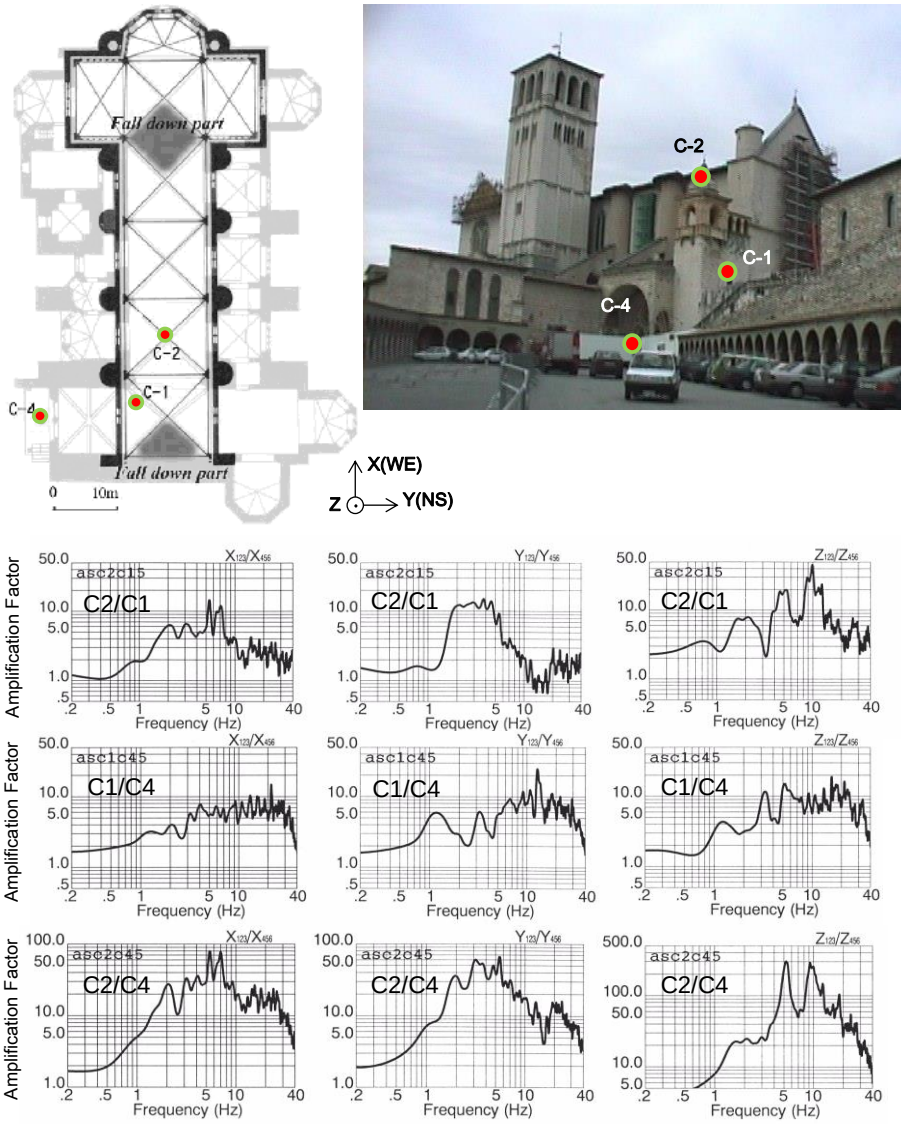

Figure 23. Earthquake response characteristics of damaged basilica

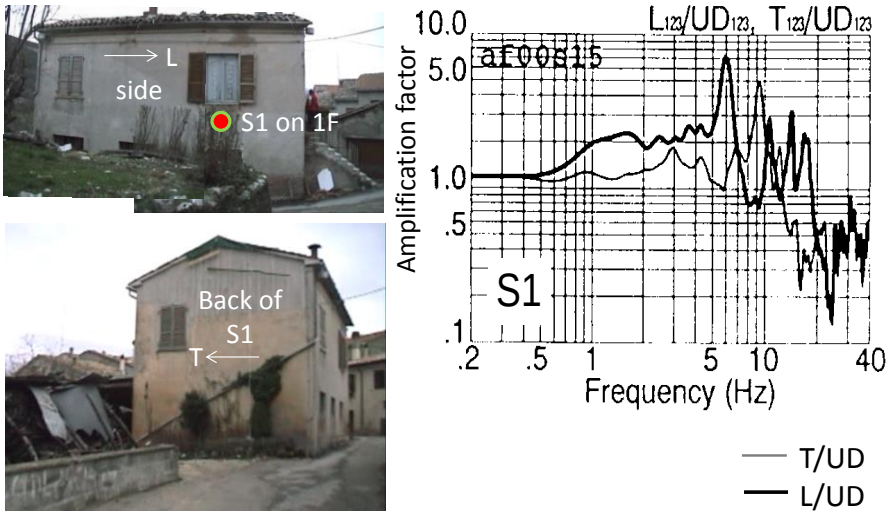

Figure 24. Earthquake response characteristics of non-damaged residence

Table 7. Kb-value, natural frequency and amplification factor for structures

	Basilica di San Francesco at Assisi	2-story house at Annifo
Fn (Hz)	2	6
A	12	7
H (m)	12	2.5
Kb (μstrain/Gal)	63	20

Note: $Kb=2500A/Fn^2/H/\pi^2$, see [8] in detail.

large as 1/100 at the basilica from the *Kb value*, it is small as 1/500 at most for the residence. It agrees that the ceiling of the basilica was collapsed but the residence was almost no damage.

The affection of the softness of the ground has usually been regarded for the building damage and grasping the characteristics of it has been concentrated. However the characteristics of ground in central Italy are generally fine. Of course the amplification characteristics of ground by earthquake motion is important, but it seems to be more important to grasp the anti-seismicity of buildings exactly and to take proper countermeasures.

It is considered to be important for public places as church to publicize the way of response against earthquake. The damage of buildings as collapse of the ceilings must be occurred at the portion

with different deformation, which is the portion concentrating the strain.

In case of *Basilica di San Francesco* in Assisi, the main axis of the structure is east-west direction and there is intersection of the entrance wall and the altar at the both side of the axis. So the structure between the entrance and the altar can swing easier to north-south direction than east-west direction. There are buttresses for reinforcement against this motion. It is clear from the result of the microtremor measurement that the structure can nevertheless swing easy in north-south direction. Because the both side around the altar and the entrance is difficult to swing in north-south direction, it is estimated that the strain was concentrated at this portion and then it caused the collapse. Thus, there are two dangerous points at the basilica and the collapse occurred at these points.

This kind of weak points will be found in the other many structures. It is considered that it will be possible to decrease human suffering by earthquake with setting a safety zone against the unexpected avoiding these weak points. Of course the function of the safety zone will be advanced with positive safeguard.

It is also important to clearly specify the safety zone to avoid evacuation wrongly for the dangerous area against the people noticing earthquake quickly and activating evacuation by alarms.

Although the ideal countermeasure is to increase the anti-seismicity of structures against expected damage, it will be possible to save a lot of human losses if it will be possible to take countermeasures to extend as much the time till collapsing a structure, even in case with difficulty to take the ideal countermeasure. Taking countermeasures for anti-seismicity and setting or constructing the safety zone are felt as urgent need.

Especially for places as churches or theaters people gathering, it is urgent task to take countermeasures against falling objects and it is required to inform dangerous area as changing structure and to take countermeasures in anticipation of the collapse.

7. Conclusions

Here investigates on the earthquake disaster prevention with strong motion records in view of damage situation of the earthquake sequence in central Italy from August 24, 2016. The result can be concluded as follows.

Although onsite EEW can be issued around one second after earthquake detection, time margin of it is only a few seconds before arrival of a large earthquake motion possibly causing damage in epicentral area with severe damage. However there are few countermeasures with such short time margin, it is important to prepare an effective way to survive and train it. It is also important to find out accurately vulnerable structures and to make them anti-seismic. It will make the time before suffering damage short and make such short time margin effective even if the damage cannot be avoided.

It is necessary to grasp properly the damaged area for quick rescue activity of suffered people. The hypocenter as a starting point of fault rupture or the magnitude of an earthquake can be determined properly about a few seconds after the first earthquake detection under the current distribution of strong motion observatories. However the hypocenter is only a starting point of fault rupture, it may discrepant from the area with severe damage in case of a large earthquake. So, here investigates how quick and proper the Max source and a crustal deformation caused by an earthquake can be estimated. As a result, the Max source can be determined within about 30 seconds, depending on a case. The permanent deformation can be also grasped with double integration of the observed waveform in a few minutes later. Therefore, it is expected whether an observation point locates close to the fault or not is cleared a few minutes after the first earthquake detection.

This research uses opened strong motion records. This kind of information are extremly important and useful for disaster prevention. Installing at least one observation station for each municipality seems to wake that the response after the earthquake dramatically quick and proper. Additionally at least important facilities would be installed own seismometer to grasp it vulnerability or to respond rationally after an earthquake.

Acknowledgement

At the time of the measurement around Assisi in 1997, Prof. Rovelli supported the authors at *Basilica di San Francesco* and villages around there and late Prof. Mucciarelli supported the authors at villages and a dam around the epicenter. The authors would like to express our gratitude for them. Especially, Prof. Mucciarelli who worked actively on the earthquake disaster prevention suddenly passed away on November 7, 2016. It is felt much regret because he was still young for further activities. The authors cannot help but feel large sense of loss. We would like to take even a part of his will for the earthquake disaster prevention. May his soul rest in peace.

All the strong motion records are opened by ITACA with support of many organizations. The authors express our thanks to these organizations.

References

[1] Yutaka Nakamura and Kenji Tomita, "*An Estimation Formula of Maximum Accerelation caused by Earthquake* (in Japanese)", Abstract Volume of the 39th Annual Meeting of JSCE, Japan Society of Civil Engineers, Vol.1, pp.785-786, October 1984.

[2] Yutaka Nakamura, "*A new Concept for the Earthquake Vulnerability Estimation and its Application to the Early Warning System*", Proceedings of Early Warning Conference, EWC'98, September 7-11, 1998, Potsdam, Germany.

[3] Jun Saita, Yutaka Nakamura, and Marco Mucciarelli, "*Relation between Seismic Damage and Dynamic Characteristics of Sub Soil -A few Examples of the 1997 Umbria-Marche Earthquake-*(in Japanese with English abstract)", Proceedings of the 10th Earthquake Engineering Symposium, Vol.1, pp.333-338, 1998.

[4] Yutaka Nakamura, "*Examination of a Rational Strong Motion Index-Relationship between the DI value and the other strong motion indeces-*(in Japanese)", Abstract Volume of the 27th JSCE, Japan Society of Civil Engineers, Earthquake Engineering Symposium, p.54, December 9-12, 2003, Osaka, Japan.

[5] Yutaka Nakamura, "*Comparison of Various Earthquake Motion Indices* (in Japanese with English abstract)", Abstract Volume of the 27th JSCE, Japan Society of Civil Engineers, Jounal of Japan Association for Earthquake Engineering, Vol.7, No.2, 2007.
[6] Yutaka Nakamura, "*The H/V Technique and Example of its Application for L'Aquila and Rome Areas*", Proceedings of the workshop DISS_10, pp.9-21, L'Aquila, 19 March 2010.
[7] Yutaka Nakamura, Tsutomu Sato, and Jun Saita, "*The 2011 off the Pacific coast of Tohoku Earthquake: Outline and some topics*", Proceedings of the workshop DISS_12, L'Aquila, 29-30 March 2012.
[8] Yutaka Nakamura, Jun Saita and Tsutomu Sato, "*Dynamic Characteristics of the Colosseum at the Pillar #40 Comparing the Results of Microtremor Measurement in 1998 and 2013*", Proceedings of the workshop DISS_15, pp.25-41, Rome, 29-30 March 2015.
[9] L. Chiaraluce, R. Di Stefano, E. Tinti, L. Scognamiglio, M. Michele, E.Casarotti, M. Cattaneo, P. De Gori, C. Chiarabba, G. Monachesi, A.Lombardi, L. Valoroso, D. Latorre, and S. Marzorati, "*The 2016 Central Italy Seismic Sequence: A First Look at the Mainshocks, Aftershocks, and Source Models*", Seismological Research Letters Volume 88, Number 3 May/June 2017.